

Antioxidant metabolism regulates CD8⁺ T memory stem cell formation and antitumor immunity

Karolina Pilipow,¹ Eloise Scamardella,¹ Simone Puccio,¹ Sanjivan Gautam,² Federica De Paoli,¹ Emilia M.C. Mazza,¹ Gabriele De Simone,¹ Sara Polletti,³ Marta Buccilli,¹ Veronica Zanon,¹ Pietro Di Lucia,⁴ Matteo Iannacone,⁴ Luca Gattinoni,² and Enrico Lugli^{1,5}

¹Laboratory of Translational Immunology, Humanitas Clinical and Research Center, Rozzano, Milan, Italy.

²Center for Cancer Research, National Cancer Institute, Bethesda, Maryland, USA. ³Humanitas University, Pieve Emanuele, Milan, Italy. ⁴Division of Immunology, Transplantation and Infectious Diseases and Experimental Imaging Center, Istituto di Ricerca e Cura a Carattere Scientifico (IRCCS) San Raffaele Scientific Institute and Vita-Salute San Raffaele University, Milan, Italy. ⁵Humanitas Flow Cytometry Core, Humanitas Clinical and Research Center, Rozzano, Milan, Italy.

Adoptive T cell transfer (ACT) immunotherapy benefits from early differentiated stem cell memory T (Tscm) cells capable of persisting in the long term and generating potent antitumor effectors. Due to their paucity ex vivo, Tscm cells can be derived from naive precursors, but the molecular signals at the basis of Tscm cell generation are ill-defined. We found that less differentiated human circulating CD8⁺ T cells display substantial antioxidant capacity ex vivo compared with more differentiated central and effector memory T cells. Limiting ROS metabolism with antioxidants during naive T cell activation hindered terminal differentiation, while allowing expansion and generation of Tscm cells. N-acetylcysteine (NAC), the most effective molecule in this regard, induced transcriptional and metabolic programs characteristic of self-renewing memory T cells. Upon ACT, NAC-generated Tscm cells established long-term memory in vivo and exerted more potent antitumor immunity in a xenogeneic model when redirected with CD19-specific CAR, highlighting the translational relevance of NAC as a simple and inexpensive method to improve ACT.

Introduction

Adoptive T cell transfer (ACT) immunotherapy of antitumor T cells redirected with chimeric antigen receptors (CARs) or T cell receptors (TCRs) revolutionized cancer treatment. Indeed, ACT as well as checkpoint inhibitor therapy definitively demonstrated that the immune system can effectively reject established tumors. Infusion of CAR-transduced T cells recognizing CD19 (CART19) is now approved by the FDA as a treatment for relapsed/refractory acute lymphoblastic leukemia and diffuse large B cell lymphoma, while CAR T cells specific for additional targets are currently being explored against other hematological malignancies and solid tumors (1). However, not all patients respond to treatment, mainly because of the development of resistance due to the loss of the CD19 expression (2) or because they receive T cells with poor functional capacity (3). Potent ACT depends on many characteristics, including the capacity of transferred T cells to mediate robust effector functions and to persist long-term (4–10). This has been shown in multiple instances to be dependent on the differentiation state of T cells in the infusion product: early differentiated stem cell memory T (Tscm) and central memory T (Tcm) cells retain a network of transcription factors and metabolic regulators that are responsible for their heightened longevity (11), superior reconstitution capacity (7, 12, 13), and enhanced antitumor responses (7, 14) when compared with committed effector memory (Tem) and terminal effector T (Tte) cells. However, Tscm cells are rare in the peripheral blood of healthy individuals and cancer patients, so new strategies have been devised for their generation by modulating the differentiation of uncommitted naive T (Tn) cell through inhibitors of GSK-3 β (7), AKT (15, 16), and BET bromodomain (17); cytokine cocktails alternative to IL-2, such as IL-7 and IL-15 (18, 19) and IL-21 (20, 21); curtailed T cell receptor signaling (22); Notch-mediated stimulation (23); and metabolic modulators (24) (reviewed in ref. 25).

A number of reports in the past few years have demonstrated that cellular metabolism is implicated in CD8⁺ T cell differentiation. Quiescent CD8⁺ Tn and memory cells rely on fatty acid oxidation (FAO)

License: This work is licensed under the Creative Commons Attribution 4.0 International License. To view a copy of this license, visit <http://creativecommons.org/licenses/by/4.0/>.

Authorship note: KP and ES contributed equally to this work.

Conflict of interest: The Laboratory of Translational Immunology receives reagents in kind from BD Biosciences as part of a collaborative research agreement.

Submitted: May 23, 2018

Accepted: August 7, 2018

Published: September 20, 2018

Reference information:

JCI Insight. 2018;3(18):e122299.

<https://doi.org/10.1172/jci.insight.122299>.

insight.122299.

to fuel the oxidative phosphorylation to meet their energy demands (26–29). Upon activation, a metabolic switch to glycolysis occurs in order to support rapid cell growth, proliferation, and effector functions (30). Modulation of the metabolic status, such as by inhibiting glycolysis (24), by favoring L-arginine (31) or cholesterol metabolism (32) or by inducing mitochondrial fusion, which, in turn, induces metabolic reprogramming (33), has been exploited in culture and in vivo to generate CD8⁺ T cells with more potent antitumor functions upon ACT. Similarly, memory-precursor CD8⁺ T cells display low mitochondrial membrane potential ($\Delta\Psi_m$), which allows selection of those cells with enhanced stemness and capacity to reject established B16 melanoma (34). The low levels of ROS found in $\Delta\Psi_m^{\text{lo}}$ T cells suggest protection from apoptosis, but there is evidence that ROS also regulate signaling pathways in multiple cell types, including T cells. In fact, CD4⁺ T cells incapable of producing ROS due to a deletion of *Uqcrcsfl*, a mitochondrial complex III subunit required for transferring electrons during respiration, fail to proliferate and differentiate into effectors (35). The rapid rise in ROS production following T cell activation also induces an antioxidant endogenous response mediated by reduced glutathione (GSH), the most abundant cellular antioxidant, that buffers excessive damage and is required for the optimal activation of mTOR (36). In fact, lower levels of GSH due to genetic ablation of *Gclc*, the catalytic subunit of glutamate cysteine ligase involved in GSH biosynthesis, results in T cell deletion as a consequence of the incapability of T cells to fuel the metabolic demand required after activation (36). These data indicate a complex regulation of the redox system during T cell activation that is important for protecting T cells from excessive damage and cell death, but whether it is required for memory T cell specification is at present unknown.

We provide evidence that circulating human CD8⁺ Tn and Tscm cells display a substantial reservoir of reduced GSH ex vivo and that scavenging ROS with antioxidants in activated CD8⁺ Tn cells blocks terminal differentiation, while allowing proliferation and generation of long-lived memory T cells with stem cell-like characteristics at the phenotypic, molecular, functional, and metabolic level. The generated Tscm cells are further shown to preferentially self-renew following adoptive transfer in syngeneic and xenogeneic models and, when redirected with a clinical-grade CD19 CAR, to mediate prolonged tumor control.

Results

Early differentiated human CD8⁺ T cells display a substantial antioxidant phenotype. Gene expression profiles change considerably during peripheral CD8⁺ T cell differentiation (10). We thus reasoned that the identification of gene signatures characterizing specific subsets would give the opportunity to mine pathways that are responsible for effector and memory differentiation from uncommitted precursors. To this aim, we retrospectively performed gene set enrichment analysis (GSEA) on publicly available gene expression microarrays of sorted human CD8⁺ Tn, Tscm, Tcm, and Tem cell populations from the peripheral blood of healthy donors (7). In accordance with their early differentiated phenotype, Tn and Tscm cells were preferentially enriched in multiple genes sets involved in mitochondrial metabolism and electron transport chain, while these cells were not enriched in gene sets related to cytotoxicity or inflammatory pathways, such as IL-12 pathways, AKT pathways, or pathways in response to IFN- γ , among others (Supplemental Table 1; supplemental material available online with this article; <https://doi.org/10.1172/jci.insight.122299DS1>). In addition, we identified that of glutathione-derived metabolic process to be significantly enriched in Tn and Tscm versus Tem cells (Figure 1A). The differentially expressed genes (DEGs) contained in this gene set, in addition to others that were manually selected, have a role in the detoxification of products of oxidative stress, such as peroxiredoxin 1 (*PRDX1*) and *PRDX5*, which are both intracellular sensors of hydrogen peroxide; nuclear factor erythroid 2 like 1 (*NFE2L1*), which regulates the expression of enzymes involved in glutathione synthesis; and different members of glutathione S-transferase family, including *GSTA1*, *GSTM3*, *GSTM2*, and *GSTM5*, which possess glutathione conjugating activity (Figure 1B). These results suggest that early differentiated CD8⁺ Tn and Tscm cells might preferentially rely on glutathione for their antioxidant activity. We next tested whether this differential gene expression program also reflects a diverse content of GSH. We stained peripheral blood mononuclear cells (PBMCs) from healthy individuals with a panel of fluorescently conjugated mAbs, directed to recognize the major subsets of naive and memory CD8⁺ T cells, and with the fluorescent probe monochlorobimane (mBCI), which reacts with GSH, and found that Tn cells retain the highest levels of this metabolite (Figure 1, C and D). The level of GSH decreased progressively with CD8⁺ T cell differentiation, where terminal effector (Tte) CD8⁺ T cells had the lowest amount (Figure 1, C and D). Thus, CD8⁺ Tn and, a lesser extent, Tscm cells retain a substantial reservoir of GSH.

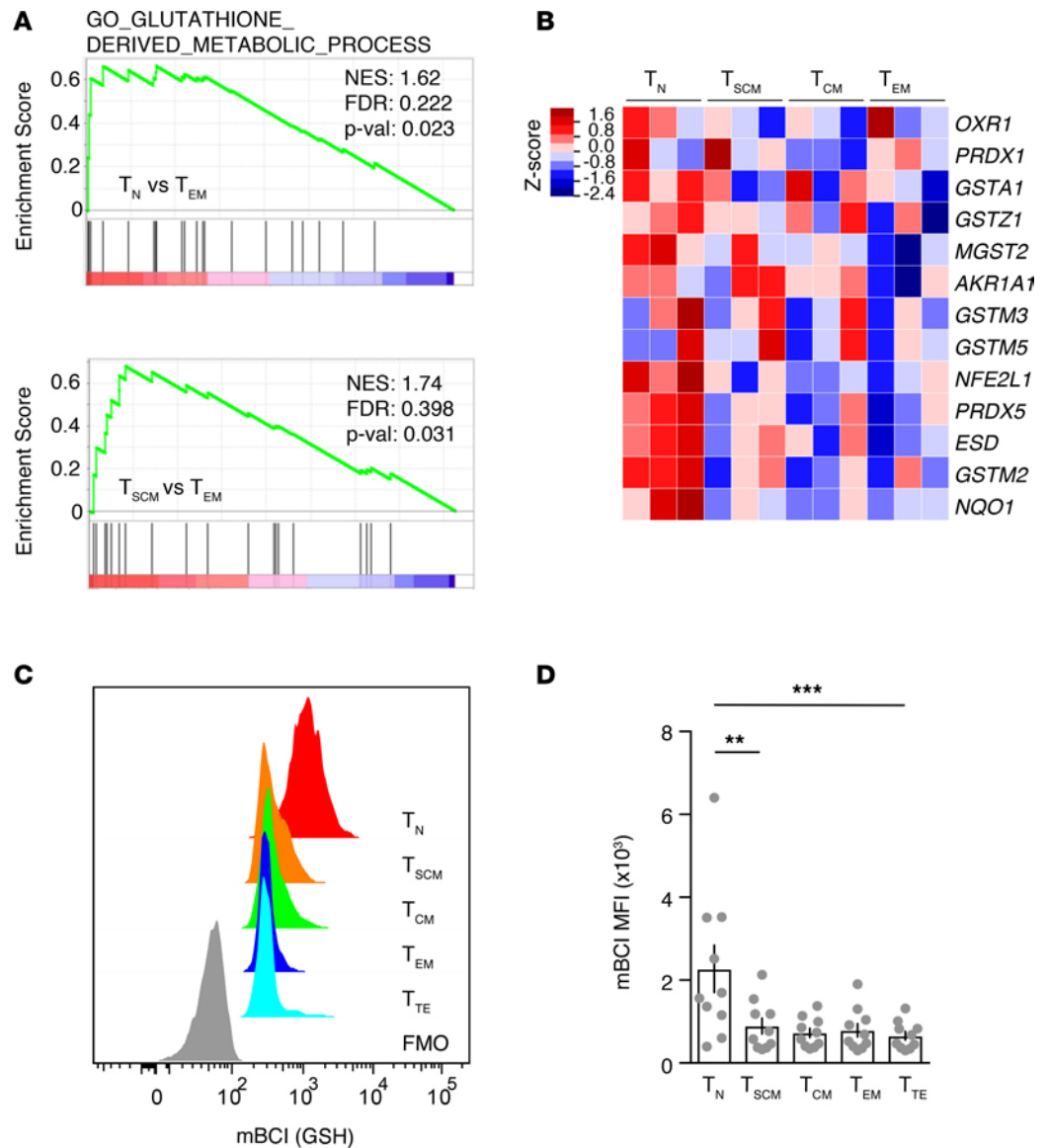


Figure 1. Early differentiated human CD8⁺ T cells display a substantial antioxidant phenotype. (A) Gene set enrichment analysis (GSEA) of glutathione-derived metabolic process signature (gene ontology c5.pb.v6.1) in T_N versus T_{EM} and T_{SCM} versus T_{EM} CD8⁺ T cells. Net enrichment score (NES) values are shown. (B) Relative gene expression level of transcripts involved in the antioxidant response in T_N , T_{SCM} , T_{CM} , and T_{EM} CD8⁺ T cell subsets from $n = 3$ HD. (C) Representative FACS analysis of GSH levels (mBCI staining) in gated CD8⁺ T cell subsets from the peripheral blood of a healthy individual. (D) Mean \pm SEM of mean fluorescence intensity (MFI) data, obtained as in C ($n = 10$). HD, healthy donor; mBCI, monochlorobimane; FMO, fluorescence minus one control. In D statistical analysis was performed with parametric 1-way ANOVA test with Bonferroni post test. ** $P < 0.01$, *** $P < 0.001$.

Modulating ROS levels regulates effector and memory CD8⁺ T cell differentiation in vitro. ACT immunotherapy of cancer benefits from early differentiated memory CD8⁺ T cells, which display superior antitumor activity, owing to their enhanced capacity to self-renew and to simultaneously differentiate into potent effectors (8, 10). T cell expansion in vitro, required to obtain sufficient numbers of T cells to be transferred, is inevitably associated with terminal differentiation; therefore, more efficient protocols capable of preserving the early differentiated state are needed. Our results illustrated in Figure 1 suggest that favoring the antioxidant capacity in activated CD8⁺ T cells could arrest effector differentiation while promoting an early differentiated memory phenotype. To test this, we sorted human peripheral blood CD8⁺ T_N cells from healthy donors and activated them with anti-CD3/CD28 antibody-conjugated beads in the presence of human IL-2 and IL-12 (hereafter referred to as control [CTRL]). We have recently reported that this treatment generates a

large pool of highly proliferating T cells with a bona fide effector phenotype (22). In order to modulate the ROS levels in culture, we tested a panel of well-known antioxidants, including N-acetylcysteine (NAC), reduced GSH, vitamin C (vitC), and Apocynin (Apo) (Figure 2A) and evaluated the differentiation phenotype and the proliferative capacity of activated T cells at day 8 by CCR7 and CD45RO expression and by CFSE dilution, respectively. Addition of NAC, GSH, and Apo but not vitC to the culture condition blocked ROS production (Supplemental Figure 1) and the generation of Tem cells, while favoring the accumulation of early differentiated memory T cell phenotypes (Figure 2A). These molecules had variable effects on the intracellular GSH content (Supplemental Figure 1). Of note, only NAC induced T cells with a CCR7⁺CD45RO⁻ phenotype reminiscent of Tn and Tscm cells (Figure 2A) (10) while simultaneously allowing substantial proliferation (Figure 2, B and C). In this regard, proliferation of activated Tn cells was in part inhibited with 40 mM NAC and completely inhibited with 80 mM NAC (Supplemental Figure 1A). Interestingly, vitC had the opposite effect on memory phenotypes and tended to increase, rather than scavenging total ROS, at 48 hours after activation (Supplemental Figure 1B), thereby suggesting that increasing ROS levels may favor terminal differentiation (see below). For such capacity to induce Tscm phenotype cells, we decided to employ NAC for the rest of our study.

NAC serves as a broad antioxidant by providing precursors for GSH biosynthesis or by scavenging ROS directly (37). First, we evaluated the oxidative status of NAC-treated cells with specific fluorescent probes. We measured GSH levels shortly after activation by mBCI and found a significant increase at 18 hours, with a decrease in total cellular ROS (as measured by CellROX) at 18 hours (Supplemental Figure 1C) and 48 hours (data not shown) compared with CTRL. At the end of the culture period, i.e., at day 8, NAC-treated cells were similarly characterized by substantially lower total cellular ROS, mitochondria-derived anion superoxide (O₂⁻, as measured with MitoSOX), and $\Delta\Psi_m$ (as evaluated by TMRM) (Figure 2D). Such a metabolic profile has been recently associated with cell stemness (34). Further immunophenotypic characterization of NAC-treated CD8⁺ T cells revealed decreased but detectable surface expression of CD95 and increased expression of CD45RA, CD27, and CXCR3 compared with CTRL (Figure 2F), indicating bona fide Tscm cell differentiation (Figure 2G). We next asked whether we could in turn accelerate the terminal differentiation of CD8⁺ T cells by increasing ROS levels with an inducer of radicals, i.e., menadione (MD) (38) during the expansion protocol. MD-treated CD8⁺ Tn cells displayed a significant increase in total cellular ROS as shortly as 2 hours after activation (Supplemental Figure 1D). No substantial differences in GSH levels were observed at 2 hours after activation compared with CTRL cells (Supplemental Figure 1D). In line with our hypothesis, we observed that MD increased the frequency of Tem phenotype cells (in spite of Tcm phenotype cells) to more than 80% compared with about 60%, as found in the CTRL cells (Figure 2, E and G). These cells displayed a homogeneous CD45RA⁻CD27⁻CD95^{bright}CXCR3^{int} phenotype (Figure 2F), consistent with their enhanced effector differentiation.

CD8⁺ T cells acquire different cytokine production profiles during progressive differentiation, where less differentiated cells secrete mainly IL-2 and TNF and those that are more differentiated secrete mainly IFN- γ (10). To further confirm differences in effector and memory fates at functional level, cells treated for 8 days with either NAC or MD in addition to CTRL condition were restimulated with phorbol 12-myristate 13-acetate (PMA) and ionomycin and subsequently analyzed for their intracellular cytokines production. In accordance with their early differentiated phenotype, NAC-treated CD8⁺ T cells had decreased IFN- γ and increased IL-2 production compared with CTRL (Figure 2H). As Tscm cells have shown a reduced capacity to produce IFN- γ compared with more differentiated subsets, we gated on Tscm cells and found that NAC also decreased IFN- γ production in these cells (Supplemental Figure 2, A and B), thereby indicating that NAC does not only shape the frequency of T cell subsets in the final product, but also acts directly on Tscm cells to limit effector differentiation. Analysis of combinatorial cytokine expression revealed that IL-2 was produced alone or in combination with TNF (Figure 2I). On the contrary, MD repressed both IFN- γ and IL-2, but not TNF, production (Figure 2H). Residual functional capacity of MD-treated cells was mainly characterized by a combination of IFN- γ and TNF, a feature of highly differentiated effector CD8⁺ T cells (Figure 2I). In conclusion, buffering ROS production by antioxidants during T cell activation limits effector differentiation while allowing T cell expansion and generation of early differentiated T cells with a Tscm phenotype and functional profile. Instead, increasing ROS levels induces terminal differentiation.

NAC establishes a gene expression signature of long-lived memory T cells. In order to further understand the molecular insights by which NAC exerts its effects, we performed analysis of the whole transcriptome by RNA sequencing (RNAseq). As shown in volcano plot, we identified 1,997 DEGs between

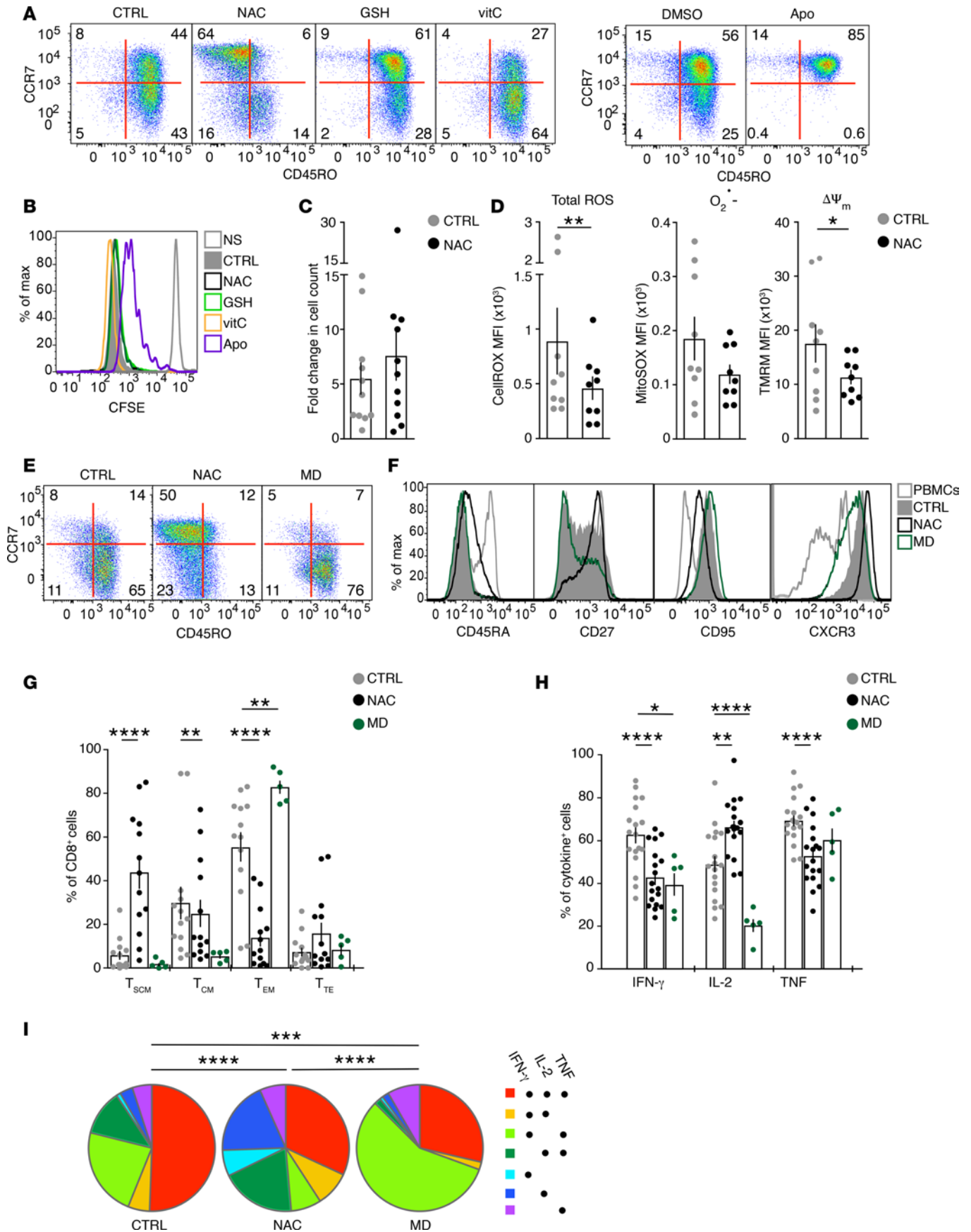


Figure 2. Modulating ROS levels regulates effector and memory CD8⁺ T cell differentiation in vitro. (A) Representative FACS analysis of CCR7 and CD45RO expression in circulating CD8⁺ Tn cells activated with anti-CD3/28, IL-2, and IL-12 in the presence of N-acetylcysteine (NAC), reduced glutathione (GSH), vitamin C (vitC), or apocynin (Apo) for 8 days. Treatments were supplemented daily. Additional DMSO control for Apo is shown. Similar data were obtained from $n = 8$ HD in $n = 4$ experiments (exp.) (NAC) and $n = 3$ HD in $n = 1$ exp. (GSH, vitC, Apo). (B) Representative histogram of CFSE dilution of cells cultured, as in A. NS, CFSE-stained, nonproliferating control cells. (C) Fold change (mean \pm SEM) in cell counts compared with baseline ($n = 11$ HD, $n = 6$ exp.) and (D) MFI (mean \pm SEM) of CellROX, MitoSOX, and TMRM ($n = 9$ HD, $n = 4$ exp.) indicative of total ROS levels, $O_2^{\cdot-}$, and $\Delta\Psi_m$, respectively, in CTRL and NAC-treated Tn cells at day 8 of culture, treated as in A. NAC was replaced every 3 days. (E) Representative CCR7 and CD45RO expression, as detected by FACS, of Tn cells activated as in A. NAC and menadione (MD) were replaced every 3 days. (F) FACS analysis of CD45RA, CD27, CD95, and CXCR3 by cells cultured, as in E. PBMCs from a HD are depicted as additional staining control. (G) Proportion (mean \pm SEM) of CD8⁺ T cells with the Tscm, Tcm, Tem, and Tte phenotypes (gated as in Methods) after culture in the indicated conditions (CTRL, $n = 13$; NAC, $n = 13$; MD, $n = 5$ from $n = 7$ [NAC] and $n = 2$ [MD] exp.). (H) Percentage (mean \pm SEM) of cytokine production in response to PMA/ionomycin stimulation by cells cultured, as in G (CTRL and NAC, $n = 18$; MD, $n = 5$ from $n = 9$ [NAC] and $n = 2$ [MD] exp.). (I) Pies depicting combinations of cytokine production obtained after stimulation, as in H. In all figures showing FACS dot plots, numbers indicate the percentage of cells identified by the gate. Statistical analyses were performed with nonparametric paired Wilcoxon (C, D, G, and H) and permutation (I) tests. * $P < 0.05$, ** $P < 0.01$, *** $P < 0.001$, **** $P < 0.0001$.

NAC-treated and CTRL CD8⁺ T cells, of which 902 were downregulated and 1,095 were upregulated (Figure 3A). Manual clustering of these DEGs according to their molecular function revealed that many genes encoding for transcription factors (TFs) involved in the effector differentiation, such as *IRF4*, *BATF*, *EOMES*, *ID2*, *PRDM1*, and components of the AP-1 complex (i.e., *FOS* and *JUN* family members), were downregulated by NAC (Figure 3B). In line with the results reported in Figure 2H showing decreased ability of NAC-treated cells to produce IFN- γ , *TBX21* (encoding T-bet), a transcriptional regulator of IFN- γ production, was repressed upon NAC treatment. In addition, multiple effector transcripts, such as granzymes (*GZMA*, *GZMB*, *GZMH*, and *GZMK*), chemokines (*CCL1*, *CCL3*, *CCL4*, and *CCL22*), and cytokines (*IFNB1* and *IFNG*), were similarly decreased (Figure 3, B and D). This was accompanied by a generalized decrease in T cell activation and exhaustion, as evidenced by lower levels of *IL2RA*, *CD40*, and *ICOS* and *HAVCR2* (TIM-3), *LAG3*, and *CTLA4* expression, respectively. Along this line, the pattern of surface molecules involved in tissue migration changed considerably upon NAC treatment. Indeed, multiple adhesion molecules and chemokine receptors generally overexpressed by effector cells (e.g., *ITGA6*, *ITGA3*, *CCR1*, and *CCR3*) or associated with homing to nonlymphoid tissues (e.g., *CCR5*, *ITGAE*, *CCR4*, and *CXCR6*) were decreased in favor of augmented *PECAM1* (encoding CD31), *CXCR3*, and *CCR7*, whose expression is a feature of early differentiated memory T cells (10). Likewise, we observed elevated levels of the master regulators of T cell persistence *TCF7* (encoding TCF-1), *LEF1*, and *ID3*; the costimulatory molecule *CD27*; and effector molecules *CCL25*, *GZMM*, and *CCL5* (encoding RANTES). Some of the differentially expressed transcripts were further validated either by RT-qPCR (*LEF1*, *TCF7*, and *PRDM1*; Figure 3C) or by flow cytometry analysis (TCF-1, TIM-3, T-bet, and GZMB; Figure 3D). We found decreased expression of heterogeneous nuclear ribonucleoprotein L-like gene (*HNRNPLL*), an enzyme that is responsible for the alternative splicing of CD45 following T cell activation (Figure 3E) (39), thus explaining the CD45RA^{+/int}CD45RO⁻ phenotype observed in Figure 2.

Increased activity of the mammalian target of rapamycin (mTOR) supports effector differentiation at the expense of long-lived memory CD8⁺ T cell development (40), and signaling downstream of mTOR is induced by oxidative stress through activation of the mTOR effector S6K1 (41). Quiescent Tn cells are characterized by low mTOR activity, which increases upon T cell activation (42). We found the mTOR signaling pathway to be downmodulated by NAC when compared with CTRL, as revealed by GSEA (Figure 3F). Accordingly, the frequency of CD8⁺ T cells with detectable phosphorylation of S6 protein on mTOR-dependent site Ser240/244 by flow cytometry was decreased after 8 days of treatment with NAC compared with CTRL (Figure 3G), further confirming the early differentiated memory-like transcriptional program induced by NAC. Generalized inhibition of T cell activation, cytotoxic molecule expression, and mTOR function could raise the question of whether NAC acts as a broad immunosuppressant, albeit still allowing T cell proliferation (Figure 2, B and C), thus possibly limiting in vivo applications such as ACT immunotherapy. To test the reversibility of the treatment, NAC-generated CD8⁺ Tscm cells were restimulated with plate-bound anti-CD3 and soluble anti-CD28 mAbs in the absence of NAC for 30 minutes, and we found that they phosphorylated S6 at Ser240/244 at levels comparable to CTRL (Figure 3G). Similar data were obtained at a second mTOR-dependent site, i.e., at Ser235/236 (Supplemental Figure 2C). Accordingly, NAC-treated cells did not display defects in T cell activation, as evidenced by the rapid upregulation of CD69 and CD25 in response to restimulation (Supplemental Figure 2, D and E).

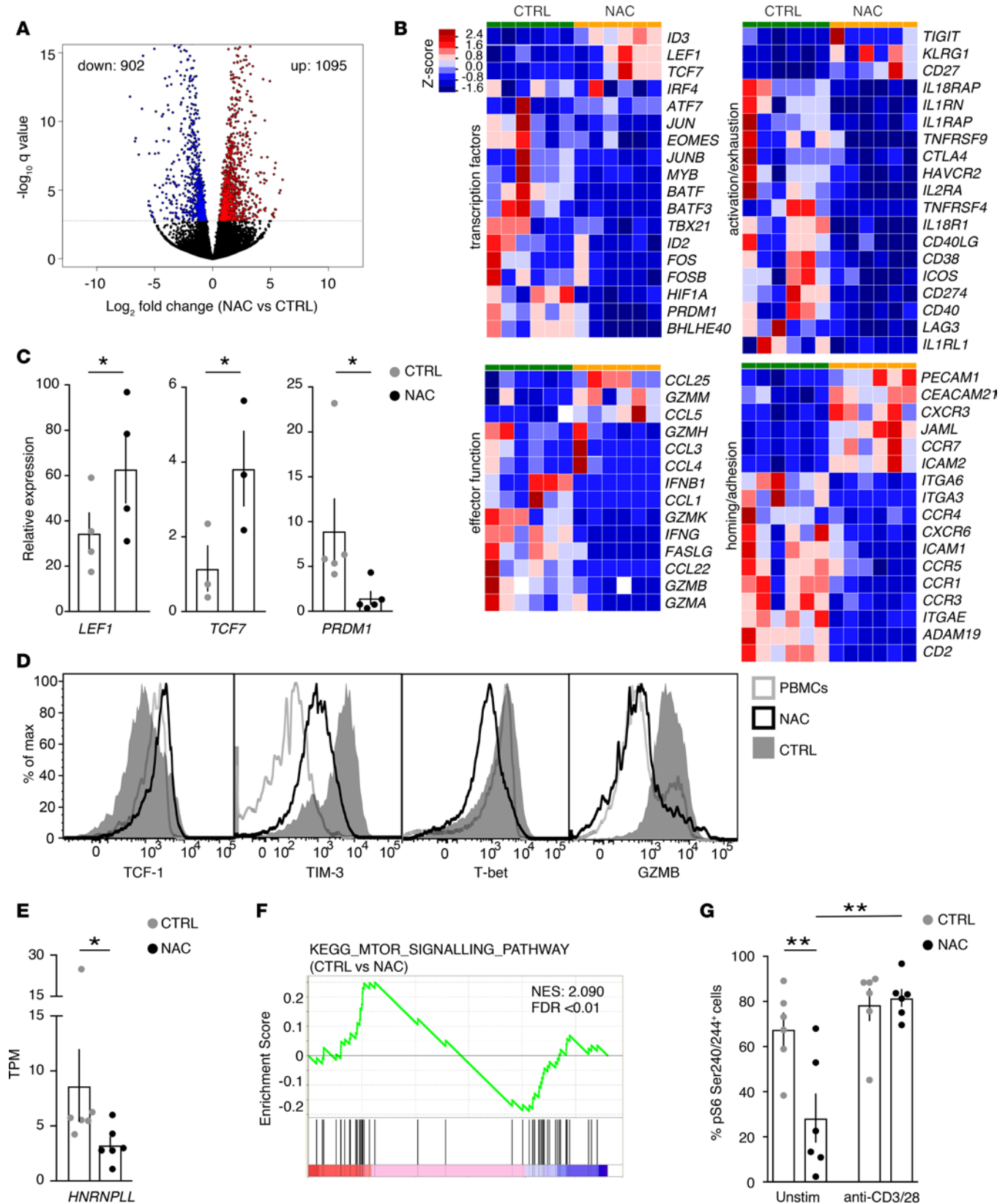


Figure 3. NAC establishes a gene expression signature of long-lived memory T cells. (A) CD8⁺ Tn cells ($n = 6$) were activated in the absence (CTRL) or presence of NAC, as in Figure 2E, and their transcriptome was analyzed by RNAseq. Volcano plot representation of differentially expressed genes (DEGs) between NAC-treated and CTRL CD8⁺ T cells with a \log_2 fold change >1 and adjusted $P < 0.05$ (q value). (B) From left to right (top): relative expression level of TFs or activation/exhaustion related genes in CTRL versus NAC-treated samples; from left to right (bottom): relative expression level of effector function or homing/adhesion-related genes in CTRL versus NAC-treated samples. (C and D) Validation of selected RNAseq transcripts, as determined by

qPCR (**C**; $n = 3$ –5 HD in $n = 2$ –3 exp.) or by FACS (**D**; similar data were obtained from $n = 3$ more HD). In **D**, a representative staining in PBMCs is depicted as an additional control. (**E**) Transcripts per million (TPM) (mean \pm SEM) of *HNRNP35* gene, as obtained from RNAseq data, as in **A**. $*P < 0.05$, paired Student's *t* test. (**F**) Gene set enrichment analysis (GSEA) of mTOR signaling pathway (c2.cp.kegg.v6.1) between CTRL and NAC-treated CD8⁺ T cells from data as in **A**. (**G**) CD8⁺ Tn cells were activated in the absence (CTRL) or presence of NAC as in Figure 2E and then washed and restimulated with anti-CD3/28 for 30 minutes or left unstimulated. The bar graph shows the (mean \pm SEM) frequencies of Ser240/244 pS6⁺ T cells ($n = 6$ HD from $n = 2$ exp.). Statistical analyses were performed with parametric paired Student's *t* test (in **C** for *LEF1* and *TCF7* expression and **E** and **G**). In **C**, significance of *PRDM1* expression was evaluated with nonparametric Wilcoxon test. $*P < 0.05$, $**P < 0.01$.

NAC induces metabolic reprogramming in generated CD8⁺ Tscm cells. It is well known that mTOR regulates multiple metabolic processes, including glycolysis in T cells (43). Therefore, we reasoned that inhibition of mTOR due to NAC would result in the simultaneous decrease of glycolytic activity. Indeed, we found the glycolytic pathway to be negatively associated with NAC-treated cells compared with CTRL cells at the transcriptional level (Figure 4A). Specifically, this was due to lower expression of *GAPDH*, *ENO2*, *PKM*, and *LDHA* glycolytic transcripts (Figure 4B), while others remained unchanged (data not shown). In line with these data, cells cultured in the presence of NAC were characterized by slightly lower glucose utilization from the extracellular milieu, as revealed by the decreased uptake of the fluorescent glucose analog 2-NBDG (Figure 4, C and D).

It has been shown that effector-to-memory CD8⁺ T cell conversion requires a metabolic switch from glycolysis to fatty acid oxidation (FAO), which in turn is required for survival and for recall response after reinfection (28, 29). Memory CD8⁺ T cells do not use extracellular-derived fatty acids (FAs) to fuel oxidative phosphorylation, rather they rely on FAs stored in intracellular lipid droplets that are preferentially mobilized by the activity of lysosomal-active lipase (LAL) (44). Accordingly, NAC-induced Tscm cells showed lower uptake of FAs from the extracellular milieu (Figure 4, C and E) and increased levels of carnitine palmitoyltransferase 1a (*CPT1a*) gene, the main rate-limiting transporter of FAs from cytoplasm into mitochondria, compared with CTRL cells (Figure 4F), further supporting the hypothesis that FAO is preferentially active in this culture condition. Furthermore, according to published data (44), *LIPA* transcripts (encoding LAL) were significantly upregulated by NAC treatment (Figure 4G), while other lipases involved in lipid metabolism that were detected in CD8⁺ T cells, such as *G0S2*, *NCEH1*, *FABP5*, and *PLA2G16*, were significantly downmodulated, suggesting they are not involved in mobilization of intracellular FAs. We next tested whether inhibition of LAL by orlistat, a lipase inhibitor, incubated along with NAC could inhibit the generation of stem cell–like memory CD8⁺ T cells, as previously reported for murine memory CD8⁺ T cells (44). We limited orlistat treatment to 4 days after activation of CD8⁺ Tn cells to avoid toxicity and then kept cells in NAC alone for 3 additional days. Orlistat did not block, but slightly potentiated, NAC inhibition of differentiation, as evaluated by flow cytometry of surface immunophenotypes (Figure 4H). Rather, orlistat blocked IFN- γ , TNF, and, to a lesser extent, IL-2 production by NAC-generated CD8⁺ Tscm cells, while it was not effective on CTRL cells (Figure 4I), leading us to conclude that CD8⁺ Tscm cells rely on intracellular FAs metabolism for their effector functions rather than for long-lived memory T cell formation.

NAC promotes stem cell–like memory CD8⁺ T cell formation and potent antitumor immunity in vivo. We have demonstrated that limiting ROS production during human effector T cell activation generates early differentiated memory T cells with Tscm phenotype and functionality. The gene expression profile of these cells suggests long-term self-renewing capability, which we further investigated in relevant xenogeneic and syngeneic mouse models in vivo. First, CTRL effector cells and NAC-generated Tscm cells, differentiated in vitro, as in Figure 2E, were adoptively transferred into NOD/SCID/ γ -chain knock out (NSG) mice and were evaluated at day 15 after transfer for their potential to engraft, expand, and differentiate. The two cell products acquired a homogeneous CCR7-CD45RO⁺ Tem-like progeny, irrespectively of the original phenotype, as previously described for the ACT of human T cell subsets in NSG mice (7), and featured similar, elevated expression of PD-1 and TIM-3 surface markers, both in the spleen (Figure 5A) and the lung (data not shown). In contrast, NAC-generated CD8⁺ Tscm cells expressed slightly increased Ki-67 expression, suggesting increased proliferative capacity (Figure 5, A and B). Of most importance, a larger fraction of proliferating Ki-67⁺ cells expressed TCF-1 in mice receiving NAC-treated Tscm cells compared with control effector cells (Figure 5, A and C), thus indicating that NAC programs CD8⁺ T cells for self-renewal in vivo.

Despite relevance for human applications, the xenogeneic model may be considered artificial for testing self-renewal and establishment of long-term memory. Thus, we turned to a syngeneic model, in which T cell receptor (TCR) transgenic CD8⁺ Tn cells specific for the hepatitis B virus epitope Cor93 (45) were

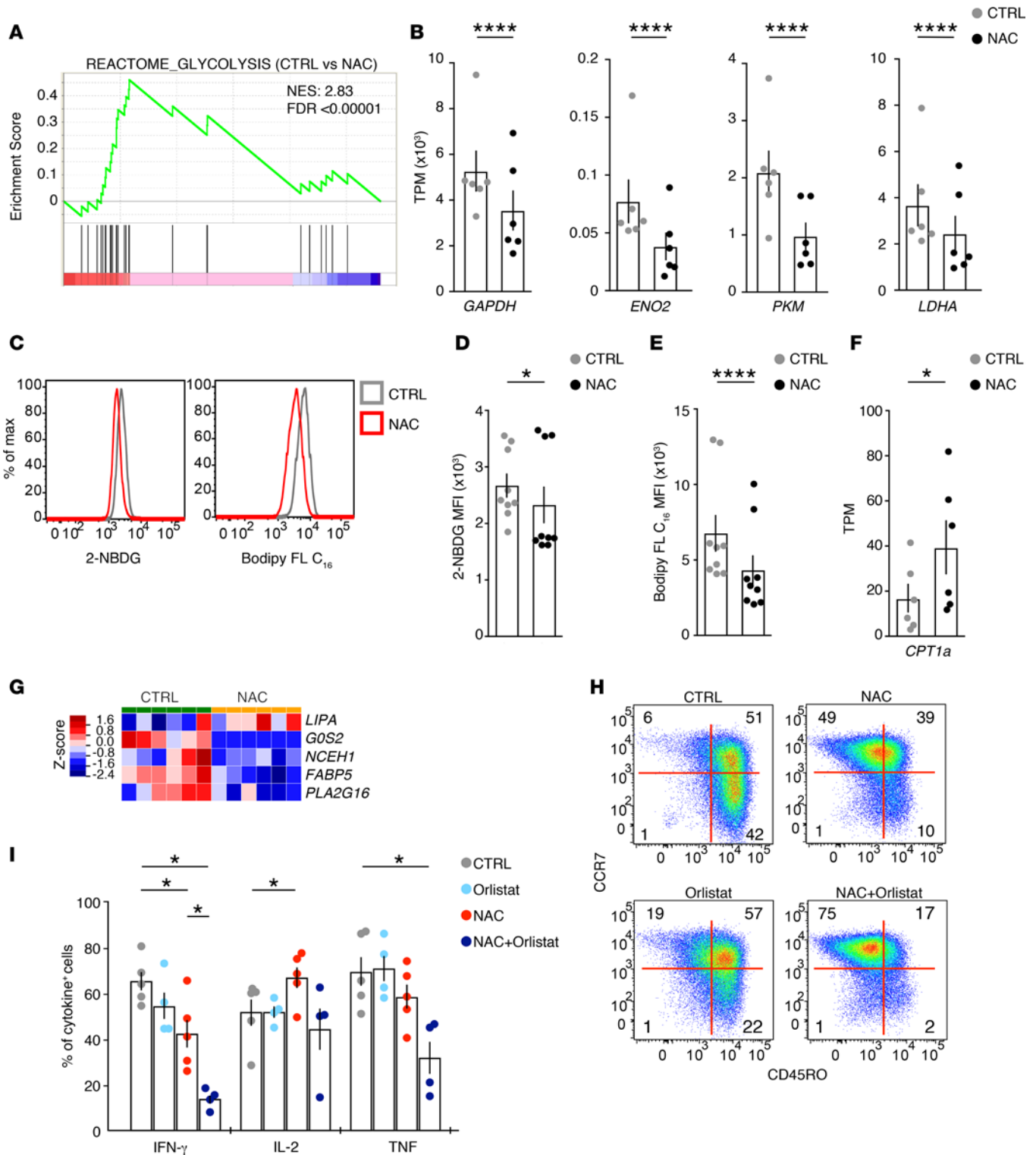


Figure 4. NAC induces metabolic reprogramming in generated CD8⁺ Tscm cells. (A) Gene set enrichment analysis (GSEA) of glycolysis signaling pathway (c2.cp.reactome.v6.1) between CTRL and NAC-treated CD8⁺ T cells activated for 8 days, as in Figure 2A, and as assessed by RNAseq, as in Figure 3A (*n* = 6). (B) Transcripts per million (TPM) (mean ± SEM) (*n* = 6) of differentially expressed glycolytic genes assessed by RNAseq, as in Figure 3A. (C) Representative FACS histograms of 2-NBDG (fluorescent glucose analog) and Bodipy FL C16 (fluorescent fatty acid synthetic precursor) uptake by CTRL and NAC-treated CD8⁺ T cells, activated for 8 days, as in Figure 2A. (D and E) Cumulative data (mean ± SEM; *n* = 9 HD, *n* = 5 exp.) of 2-NBDG (D) and Bodipy FL C16 (E) uptake, as in C. (F) *CPT1a* TPM (mean ± SEM) and (G) relative gene expression level of selected lipases in CTRL and NAC-treated CD8⁺ T cells, activated for 8 days, as in Figure 2E, and as assessed by RNAseq, as in Figure 3A (*n* = 6). (H) Representative CCR7 and CD45RO expression, as detected by FACS, in human circulating CD8⁺ Tn cells activated with anti-CD3/28, IL-2, and IL-12 in the presence of NAC, orlistat, or a combination of both. Numbers in the plots indicate the frequency of cells identified by the gates. (I) Percentage (mean ± SEM) of cytokine production in response to PMA/ionomycin stimulation by cells cultured, as in H (*n* = 5 HD in *n* = 2 exp.). Statistical analyses for B and D-F were performed with parametric paired Student's *t* test and for I with nonparametric Wilcoxon test. **P* < 0.05, *****P* < 0.0001.

purified from uninfected mice and activated *in vitro* with the cognate peptide and high-dose IL-2 in the presence or absence of NAC for 8 days, followed by ACT in wild-type animals. At day 35 after transfer, we recovered a higher frequency of Tn-like cells (i.e., CD62L^{hi}CD44^{lo}) in spleens and lymph nodes of mice injected with NAC-treated CD8⁺ T cells, in spite of CD44^{hi}CD62L^{hi} Tcm cells (in LNs) or CD44^{hi}CD62L^{hi} Tem cells (in spleens), as shown by representative dot plots (Figure 5D) and cumulative data from 5 mice (Figure 5G). We obtained similar data at day 5 after ACT (data not shown). The Tn-like cells expressed higher levels of CXCR3 and Sca-1 compared with endogenous CD8⁺ Tn cells (Figure 5F), thus indicating that they are postmitotic and bona fide Tscm cells, as previously described (6). As a whole, NAC-treated CD8⁺ T cells displayed lower levels of CD44 compared with CTRL cells after adoptive transfer (Figure 5E). In accordance with such increased relative frequency of early differentiated memory phenotypes and with human data, NAC-treated Cor93-specific CD8⁺ T cells produced less IFN- γ but similar amounts of TNF compared with control cells at day 35 after ACT when restimulated with the cognate peptide *in vitro* (Figure 5H). We concluded that limiting ROS metabolism favors the generation of antigen-specific Tscm cells with enhanced self-renewal capacity.

Stem cell-like properties are important correlates of antitumor T cell responses following ACT. We aimed to test whether NAC-induced Tscm cells retain such potency *in vivo*. Therefore, the specificity of these and CTRL effector CD8⁺ T cells, generated as described in Figure 2E, was redirected with a chimeric antigen receptor (CAR) recognizing the human CD19 molecule, followed by ACT of small numbers (i.e., 2.5×10^5) of cells into NSG mice bearing established CD19⁺ acute lymphoblastic leukemia cells, injected 7 days earlier as recently described (21). Mice were monitored for tumor burden on a weekly basis after ACT. Untreated mice died within 2 weeks. While mice receiving control cells had a slight survival benefit (i.e., ~20 days; Figure 5, I and J), those receiving NAC-induced Tscm cells successfully controlled tumor growth for a prolonged period of time (Figure 5I), as revealed by bioluminescent imaging of tumor cells, and experienced increased survival (Figure 5J). Two of those five mice infused with NAC Tscm cells did not have detectable leukemic cells in the body as late as 27 days after ACT (Figure 5I), thereby suggesting that they succumbed because of the potency of xenogeneic graft-versus-host disease mediated by transferred CD8⁺ T cells. In conclusion, CD8⁺ Tscm cells generated by NAC treatment display superior antitumor capacity and are suitable for ACT immunotherapy of cancer.

Discussion

We have demonstrated that the simple addition of inexpensive antioxidants to the manufacturing procedure of CD19 CAR-redirectioned T (CART19) cells inhibits effector differentiation while enabling extensive expansion and acquisition of stem cell-like CD8⁺ T cell properties at the phenotypic, functional, gene expression, and metabolic level. Among the few antioxidants tested, NAC demonstrated superior activity in this context because of its capability of inducing an abundant cell population with the naturally occurring CD45RO⁺CD45RA⁺intCCR7⁺CD95^{dim}CXCR3^{bright} Tscm cell phenotype. Increased frequency of Tscm cells at the time of collection enables reaching sufficient numbers of therapeutic T cells to be infused (46). Moreover, they are highly desired in the ACT infusion product because they are known to exert more potent antitumor immunity compared with early differentiated Tcm cells or fully differentiated cytotoxic Tem cells (3, 7, 47). This is ascribed to their enhanced capability to persist in the long-term and to differentiate into more potent effectors upon target recognition. The data presented here as well as additional studies clearly highlight the need to modify current protocols of T cell expansion, generally involving T cell receptor stimulation and high-dose IL-2, so as to preserve/induce the long-lived memory T cell signature while allowing sufficient expansion (7, 15–24).

NAC-induced CD8⁺ Tscm cells from Tn precursors *in vitro* displayed features of self-renewal following ACT *in vivo*. This is ascribed to elevated levels of TCF-1 that are maintained in actively proliferating cells. TCF-1 orchestrates the long-term repopulation capacity of early differentiated memory precursors even in the context of persistent stimulation and inflammatory conditions, such as in chronic viral infection and cancer (48). Therefore, the induction of a TCF-1⁺ memory phenotype that is actively maintained *in vivo* is beneficial for the antitumor immune response, as it provides prolonged antitumor immunity, as we observed in a xenogeneic mouse model with CD19 CAR-redirectioned Tscm cells.

Despite using an NSG model of leukemia that is devoid of endogenous immunosuppression, our findings are in line with recent data from syngeneic murine models showing that NAC enhanced anti-melanoma immunity of pmel-1 (49) and TRP-1-specific (50) CD8⁺ T cell ACT. In these studies, improved antitumor

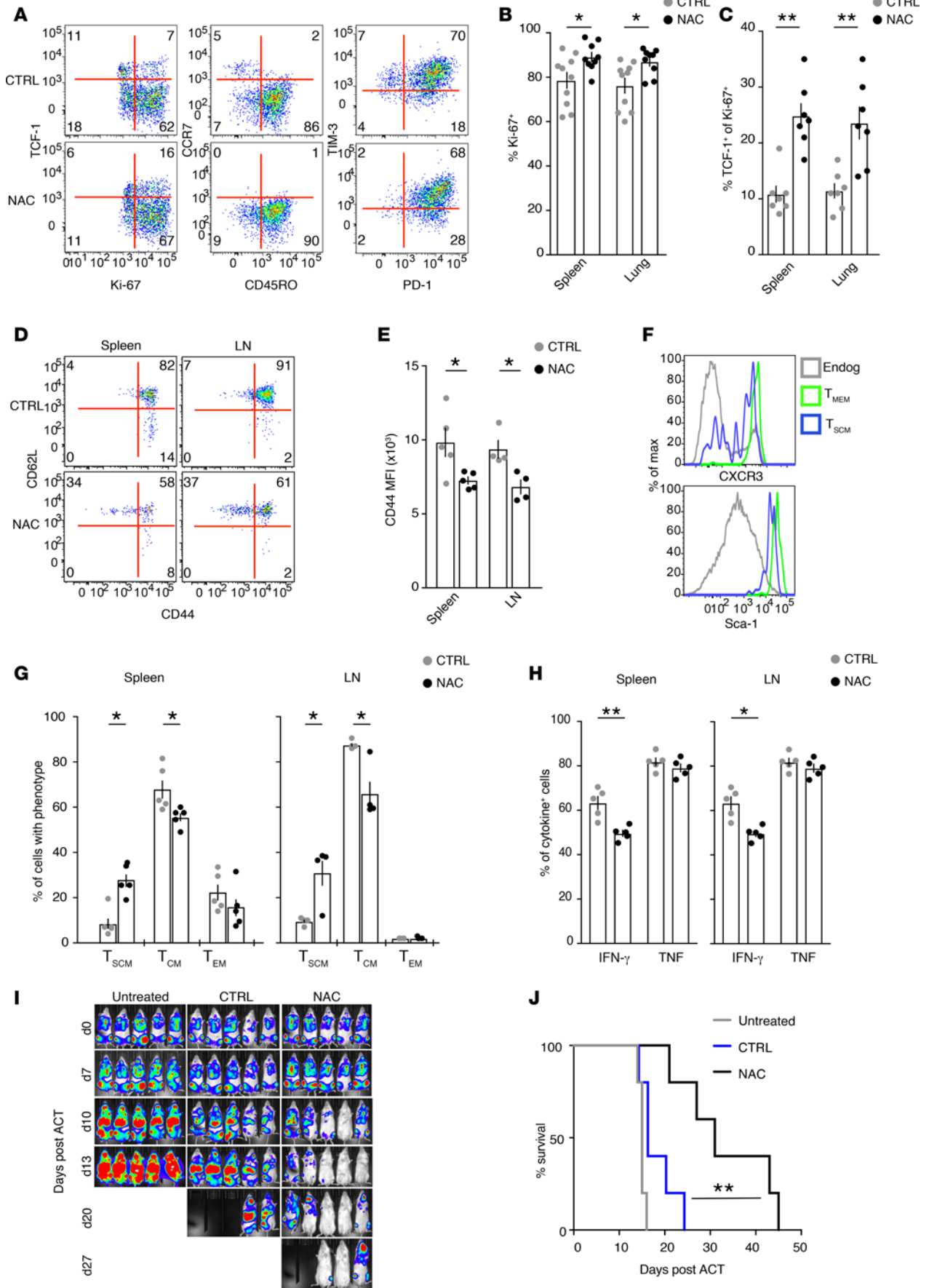


Figure 5. NAC promotes stem-like memory formation and potent antitumor immunity in vivo. (A) Representative FACS analysis of protein expression by human circulating CD8⁺ Tn cells, activated as in Figure 2A, and adoptively transferred in NSG mice. Data refer to CD8⁺ T cells isolated from spleens at day 15 after ACT. Similar data were obtained from $n = 2$ additional exp. ($n = 3$ –4 mice/group). (B and C) The ex vivo frequencies of Ki-67⁺CD8⁺ T cells (B; CTRL, $n = 10$; NAC, $n = 9$; $n = 3$ exp.) and TCF-1⁺ cells within the Ki-67⁺CD8⁺ T cell fraction (C; CTRL and NAC, $n = 7$; $n = 2$ exp.), as obtained in spleens and lungs of mice treated as in A. (D) Representative CD44 and CD62L expression in HBV Cor93-specific CD8⁺ Tn cells activated in vitro with cognate peptide and high-dose IL-2 for 8 days followed by transfer in wild-type C57/BL6 mice ($n = 5$ mice/condition in $n = 1$ exp.). Data refer to day 35 after ACT. Transferred cells were identified by the congenic marker CD45.1 while endogenous cells were CD45.2. (E) MFI (mean \pm SEM) of CD44 in CD8⁺ T cells from D. (F) Representative histograms of surface CXCR3 and Sca-1 expression by Cor93-specific CD8⁺ T cells gated as Tscm (CD44^{lo}CD62L^{hi}) or Tmem (CD44^{hi}CD62L^{hi}) cells from an animal receiving NAC-treated CD8⁺ T cells. Endogenous host CD8⁺ T cells are shown as a control. Data refer to day 35 after ACT. Similar data were obtained from $n = 4$ more mice. (G) Frequencies (mean \pm SEM) of Tscm, Tcm, and CD44^{hi}CD62L^{lo} Tem cells (gated as in D) within the Cor93-specific CD8⁺ T cells previously activated in the absence (CTRL) or presence of NAC. Data refer to day 35 after transfer ($n = 5$ mice/treatment group). (H) The frequency of Cor93-specific CD8⁺ T cells (adoptively transferred as in D) producing IFN- γ and TNF following restimulation with the cognate peptide for 4 hours ($n = 5$ /group). (I) Bioluminescence imaging of NALM-6 leukemic cells in NSG mice left untreated or adoptively transferred with human CD8⁺ Tn cells previously activated with anti-CD3/28, IL-2, and IL-12 in the absence (CTRL) or presence of NAC for 8 days and redirected with CD19 CAR ($n = 5$ mice/group). (J) Kaplan-Meier survival curve of mice treated as in H. For all FACS dot plots, numbers indicate the percentage of cells identified by the gate. Statistical analyses were performed with nonparametric Mann-Whitney test (B, C, E [LN], and G), parametric Student's *t* test (E [spleen] and H) or Mantel-Cox analysis (J). * $P < 0.05$; *** $P < 0.01$.

immunity was ascribed to inhibition of ROS-induced DNA damage and enhanced survival, rather than induction of long-term memory, as shown in the present manuscript. Despite the fact that differences between human and murine CD8⁺ T cell responses to NAC may still be at the basis of such a discrepancy, we formally demonstrated that NAC treatment before ACT favors the formation of antigen-specific CD8⁺ Tscm cells in a syngeneic mouse model, further confirming that ROS levels regulate effector and memory differentiation.

A recent genetic study in mice has shown that mitochondrial ROS are required for clonal expansion and effector differentiation of CD4⁺ T cells through NFAT induction and subsequent IL-2 secretion (35). This is coupled to an endogenous antioxidant response mediated by GSH that buffers excessive damage and is required for the optimal activation of mTOR (36). However, increased ROS production by MD to levels that are not toxic resulted in accelerated differentiation and loss of effector functions (Figure 2), while excessive ROS scavenging by NAC inhibits T cell proliferation (Supplemental Figure 1A). Overall, these data support a model where tightly controlled ROS levels balance effector and memory differentiation, while excessive or very low levels result in apoptosis and immunosuppression, respectively. This behavior is reminiscent of that of hematopoietic stem cells, where heightened ROS levels cause loss of quiescence and multipotency and rapid differentiation (51).

The exact mechanism by which NAC uncouples T cell differentiation from proliferation is not completely understood. NAC may exert its antioxidant activity in multiple ways, e.g., by scavenging ROS directly (52) and by serving as a precursor of glutathione biosynthesis, which, in turn, is involved in redox reactions and direct protein S-glutathionylation on cysteine residues (53). ROS have biological activities that extend beyond DNA damage and subsequent induction of apoptosis. They can promote the formation of disulfide bonds by oxidation and either activate or inhibit protein activity. Among these, increased signaling downstream of mTOR due to direct activation of S6K1 and HIF-1 α stabilization are observed in the presence of increased ROS (51), and we have shown that NAC has a generalized inhibitory effect on several pathways that are regulated by these molecules, including glycolysis, induction of TFs mediating terminal differentiation, and exhaustion. Removal of NAC unleashed mTOR activation and allowed effector differentiation and acquisition of potent antitumor functions in vivo (Figure 5). Therefore, metabolic capacity and activation must be restrained during culture but highly induced following ACT to support full proliferation and differentiation. It is unknown at the moment whether NAC could be infused in vivo following ACT to maintain a pool of undifferentiated T cell precursors that can serve as a reservoir of long-term immunity. However, the concern is that NAC may limit antitumor immunity by restraining T cell activation and proliferation (Figure 3 and Supplemental Figure 1, respectively).

In conclusion, modulation of ROS levels by antioxidants is a feasible and inexpensive approach to obtain stem cell–like memory T cells to be used in ACT immunotherapy. More importantly, the availability of clinical-grade NAC can allow for the rapid implementation of this strategy into T cell manufacturing protocols. It is now important to understand how the use of NAC relates to other protocols that have been developed to obtain Tscm cells (7, 15–24). Identification of a common metabolic or transcriptomic signature will lead to the identification of novel molecular targets of long-lived memory development that can further benefit antitumor immunity.

Methods

Cells. PBMCs were isolated from buffy coats from healthy donors. Preliminary experiments determined that NAC has the same effect on both fresh and thawed cells that were previously frozen in liquid nitrogen in a solution containing FBS + 10% dimethyl sulfoxide (DMSO), according to standard procedures, as described previously (18). CD8⁺ Tn cells were enriched by magnetic negative selection with the Naive CD8⁺ T cells MojoSort kit (catalog 480046, BioLegend), according to the manufacturer's instructions. Cells were used only when purity after isolation was >95%, as determined by flow cytometry analysis of CCR7, CD45RO, CD45RA, CD27, and CD95.

Polychromatic flow cytometry. Fluorochrome-conjugated mAbs were purchased from BD, BioLegend, and eBioscience (Supplemental Table 2) and titrated to determine optimal concentrations. Cells were stained with Zombie Aqua fixable viability dye (catalog 423102, BioLegend) for 15 minutes at room temperature in PBS. Surface markers were detected by incubating cells with relevant mAbs for 20 minutes at room temperature, except for chemokine receptors that were detected by incubating cells at 37°C for 20 minutes in HBSS in the presence of 2% FBS. The Cytofix/Cytoperm kit (catalog 554722/554723, BD) was used to detect intracellular cytokine expression according to the manufacturer's instructions. Fatty acid uptake was measured by incubating cells with Bodipy FL C₁₆ (final concentration: 16 nM; catalog D3821, Invitrogen) at 37°C for 30 minutes. Glucose uptake was measured incubating cells with 2-NBDG (final concentration: 150 μM; catalog 186689-07-6, Cayman) at 37°C for 5 minutes. GSH and total cellular ROS were measured by incubating cells with mBCI (final concentration: 10 μM; Invitrogen) at 37°C for 10 minutes and CellROX (final concentration: 1 μM; Invitrogen) at 37°C for 30 minutes, respectively. Mitochondrial membrane potential was measured by incubating cells with TMRM (final concentration: 0.15 μM; Invitrogen). In the case of peripheral blood samples collected from mice, red blood cells were lysed with ACK solution (made in-house; 155 mM NH₄Cl, 10 mM KHCO₃, and 0.1 mM EDTA-2Na; all from MilliporeSigma) diluted in H₂O for 5 minutes, washed twice with PBS, and stained with mAbs (Supplemental Table 2) with the same procedures mentioned above. All samples were fixed in 1% formalin for 20 minutes before acquisition on a LSR Fortessa or FACSSymphony A5 flow cytometer (BD), equipped with 4 and 5 lasers and capable of detecting 20 and 30 parameters, respectively. Flow cytometry data were analyzed and compensated with FlowJo software (version 9.9.6, FlowJo LLC) by using single-stained controls (prepared with antibody-capture beads; catalog 01-2222-42, BD), as described previously (54). Throughout the study, CD8⁺ T cell subsets were gated as follows: Tn, CD45RO⁺CCR7⁺CD27⁺CD95⁻; Tscm: CD45RO⁺CCR7⁺CD27⁺CD95⁺; Tcm, CD45RO⁺CCR7⁺; Tem, CD45RO⁺CCR7⁻; Tte, CD45RO⁺CCR7⁻.

Cell culture and treatments. Cells were cultured in complete RPMI medium supplemented with 10% FBS, 1% penicillin/streptomycin, and 2 mM L-glutamine. In all experiments, NAC (catalog A7250-50G, MilliporeSigma; final concentration: 20 mM, unless otherwise specified) was dissolved in H₂O, and pH was adjusted to 7.4 by adding NaOH. Aliquots were stored at -20°C for 1 month maximum. MD sodium bisulfite (MilliporeSigma; final concentration: 5 μM), reduced GSH (MilliporeSigma; final concentration: 4 mM), and L-Ascorbic acid (vitC, MilliporeSigma; final concentration: 100 μM) were dissolved in H₂O. Apocyanin (Apo, MilliporeSigma; final concentration: 0.4 mM) and orlistat (Cayman; final concentration: 25 μM) were dissolved in DMSO. All chemical solutions were passed through a 0.22-μm filter before use. Compounds were added to the culture medium at the time of cell seeding, titrated, and then used at the final concentrations indicated above, unless otherwise specified. Human CD8⁺ Tn cells were stimulated with Dynabeads human T-ACT CD3/CD28 (catalog 11131D Life Technologies) at a bead/cell ratio of 1:2 in 96 U-bottomed well plates for 8 days in the presence of human cytokines IL-2 (catalog 200-02-A, Peprotech) and IL-12 (catalog 200-12, Peprotech) at the final concentration of 10 ng/ml, as previously determined (22). In all experiments, medium was replaced every 3 days, unless otherwise specified in figure legends. Cell counts after culture were determined by Trypan blue dye exclusion.

Cell proliferation was determined by the analysis of the 2 μM 5-(and 6)-carboxyfluorescein diacetate succinimidyl ester (CFSE, catalog C34554, Life Technologies) dilution. In all experiments, CFSE-stained cells kept in 1 ng/ml IL-7 and IL-15 served as nonproliferating control.

To induce cytokine production, cells were plated in a final volume of 200 μl and then stimulated with PMA (final concentration: 10 ng/ml; catalog P8139, MilliporeSigma) and ionomycin (final concentration: 500 ng/ml; catalog 10634, MilliporeSigma) or left unstimulated for 3 hours at 37°C in the presence of the protein transport inhibitor GolgiPlug (final concentration: 1 μl/ml of cell culture, according to the manufacturer's instructions; catalog 555029, BD). Background cytokine production as present in the unstimulated condition was subtracted from PMA/ionomycin-stimulated cells.

To detect S6 phosphorylation at relevant sites, cells cultured in the absence or presence of NAC for 8 days were collected, washed, and restimulated in vitro with plate-bound anti-CD3 (OKT3 clone; final concentration: 5 µg/ml) and soluble anti-CD28 (CD28.2 clone; final concentration: 1 µg/ml) mAbs for 30 minutes. Cells were immediately fixed with 4% formaldehyde for 15 minutes at room temperature, washed with 1% BSA in PBS, incubated with Triton X-100 for 30 minutes at room temperature, washed twice with 1% BSA in PBS, and subsequently permeabilized for 10 minutes on ice with ice-cold methanol (50% in PBS). Cells were washed twice with 1% BSA in PBS and stained with mAbs specific for CD3, CD8, and Ser240/244 or Ser235/236 pS6 (Supplemental Table 2).

As we noted that restimulation with Dynabeads results in excessive cell death, we used anti-CD3/CD2/CD28 antibody-conjugated beads (1 bead: 2 cells; Miltenyi) for 24 hours to induce expression of activation markers CD69 and CD25, further detected by flow cytometry with fluorochrome-conjugated mAbs (Supplemental Table 2).

Real-time PCR (qPCR). Total RNA was purified with the RNeasy Micro Kit (Qiagen), retrotranscribed using the High-Capacity cDNA Reverse Transcription Kit (Applied Biosystems), and analyzed by qPCR with hydrolysis probes *LEF1* (Hs01547250_m1), *TCF7* (Hs00175273_m1), *PRDMI* (Hs00153357_m1), and *2BM* (Hs00187842_m1) as reference gene (Applied Biosystems). qPCR was performed with the Fast Real-Time PCR System (Applied Biosystems). Expression levels were normalized (ΔCt) to *2BM* endogenous control and calculated using $2^{-\Delta\text{Ct}} \times 10^3$ formula.

Microarray data analysis. Microarray probe fluorescence signals downloaded from the Gene Expression Omnibus (GSE23321) were converted to expression values using robust multiarray average procedure RMA (55) of Bioconductor Affy package. Specifically, intensity levels were background adjusted and normalized using quantile normalization, and \log_2 expression values, for a total of 20,673 custom probe sets, were calculated using median polish summarization and Entrez custom chip definition files for Human Gene 1.0 ST arrays (hugene10st_Hs_ENTREZG version 21.0.0). All data analyses were performed in R version 3.3.3 using Bioconductor libraries and R statistical packages.

Overrepresentation analysis (microarray). Overrepresentation analysis was performed using GSEA software (<http://software.broadinstitute.org/gsea/msigdb/>) (56) and Gene Ontology gene sets (c5.bp.v6.1) “GO_GLYCATION_DERIVATIVE_METABOLIC_PROCESS” from Molecular Signatures Database. GSEA was applied on \log_2 -transformed expression data of the entire data set and performed using Signal2Noise as metric and 1,000 permutations of specific gene sets.

Gene expression profiling by RNAseq. CD8⁺ Tn cells expanded in vitro were harvested at day 8, washed with PBS without Ca²⁺ and Mg²⁺, and lysed in the presence of DNase (catalog 79254, Qiagen) for subsequent total RNA purification with the RNeasy Micro Kit (catalog 74034, Qiagen). Libraries were prepared using the Nextera XT DNA Library Preparation Kit starting from 2 ng total RNA (57). Libraries were diluted to a final concentration of 2 nM and pooled (final concentration: 1.2 pM), followed by sequencing on Illumina Nextseq 500 using the NextSeq 500/550 High Output v2 kit (75 × 1 cycles, catalog FC-404-2005, Illumina).

RNAseq data analysis. After quality check using FastQC (<http://www.bioinformatics.babraham.ac.uk/projects/fastqc>), 75-bp single-end reads of $n = 6$ /condition samples (total $n = 12$) were aligned to the *Homo sapiens* reference genome (Ensembl assembly GRCh38) using STAR (version 2.5.1b) (58). Mapping was run with default parameters, and reads were counted with GeneCounts. Statistical significance of differential expression was assessed using the edgeR package (version 3.22) (59) followed by Benjamini-Hochberg multiple testing correction to estimate the FDR (FDR < 0.05). Expression data are available at Gene Expression Omnibus through accession number GSE114765.

Overrepresentation analysis (RNAseq). GSEA was applied on the entire list of genes that compose the RNA-seq expression matrix. Genes were ranked based on their \log_2 fold changes calculated by the edgeR package and then analyzed by GSEA in preranked mode with a “classic” enrichment statistic. Gene sets of interest (“KEGG_MTOR_SIGNALLING_PATHWAY” and “REACTOME_GLYCOLYSIS”) were retrieved from the C2 collection (c2.cp.kegg.v6.1, c2.cp.reactome.v6.1) of the Molecular Signatures Database.

Mice. NOD.Cg-Prkdc^{scid} IL2rg^{tm1Wjl}/SzJ (NSG) mice (Jackson Laboratories), bred in SPF conditions, both males and females at 7 weeks of age, were used for adoptive transfer experiments. Briefly, 1×10^6 NAC-induced CD8⁺ Tscm or control CD8⁺ T cells, generated as described above, were cotransferred by retro-orbital injection with 5×10^6 to 6×10^6 autologous PBMCs, previously depleted of CD8⁺ T cells by incubation with anti-CD8 APC mAb (Supplemental Table 2), followed by detection of APC by anti-APC microbeads

(Miltenyi) and negative magnetic separation with LS columns (Miltenyi), according to the manufacturer's instructions. Depletion was >99%. Mice were sacrificed 15 days after transfer. For mononuclear cell isolation, tissues were minced and filtered through a 100- μ m cell strainer, and stained with mAbs (Supplemental Table 2) as described above. To detect intracellular markers, cells were fixed and permeabilized with the FoxP3 transcription factor staining buffer kit (catalog BMS00-5523-00, eBioscience) according to the manufacturer's instructions and stained with anti-Ki-67 and anti-TCF-1/7 mAb (Supplemental Table 2).

For tumor experiments and ACT, female NSG mice were intravenously injected with 2.5×10^5 NALM6-GL cells, followed 7 days later by 2.5×10^5 CD19-CAR⁺CD8⁺ T cells expanded with Dynabeads and IL-2 and IL-12 in the presence or absence of 20 mM NAC, as described above. CAR lentiviral transduction was performed as previously described (21). Recombinant human IL-15 (obtained from the National Cancer Institute) (60) was injected intraperitoneally every other day (1 μ g per mouse). Tumor burden was measured using the Xenogen IVIS Lumina (Caliper Life Sciences), as previously described (21).

Generation of murine effector CD8⁺ T cells and adoptive transfer. Splenocytes from 9-week-old male Cor93 TCR-transgenic mice (lineage BC10.3 inbred CD45.1) (harboring a transgenic TCR specific for the HBV virus epitope Cor93) (45) were incubated with 10 μ g/ml Cor93-100 (K^b; MGLKFRQL) peptide (Primm) at 37°C for 1 hour, washed, and cultured in complete RPMI 1640 (10% FBS, 2 mM L-glutamine, 50 mM 2-mercaptoethanol, 10 mM HEPES, 100 mM nonessential amino acids, and 1% penicillin/streptomycin). In this case, NAC was used at 10 mM to avoid inhibition of proliferation. Two days later, cells were cultured in fresh medium supplemented with 2.5% EL-4 supernatant [or 20 ng/ml of recombinant IL-2 (R&D)]. Media supplemented with cytokines were replaced every 2 days. 5×10^6 CD8⁺ T cells were injected i.v. into wild-type recipient animals (C57BL/6). At day 5 or day 35 after transfer, mice were sacrificed and spleens and lymph nodes were dissected to obtain single-cell suspension according to standard protocols. Cells were then prepared for flow cytometry as described above. Alternatively, cells were plated in 96-well plates and restimulated with 10 μ g/ml Cor93-100 cognate peptide or left unstimulated in the presence of Golgi Plug (BD) for 4 hours, followed by the intracellular staining of IFN- γ and TNF, as described above.

Statistics. Analyses were performed using GraphPad PRISM version 7 and SPICE version 5.22 softwares. Heatmaps were generated based on relative expression values (Z-score) using Seaborn package (version 0.8.1). Data were first tested for normal distribution with D'Agostino-Pearson, Shapiro-Wilk, or Kolmogorov-Smirnov normality tests and then analyzed with 2-tailed Student's *t* test (parametric data) or Wilcoxon rank test (nonparametric data) when comparing two groups. One-way ANOVA with Bonferroni post test was used to compare 3 groups. Mantel-Cox analysis was performed to analyze the Kaplan-Meier survival curve. *P* values are 2 tailed; *P* values of less than or equal to 0.05 were considered significant.

Study approval. All experiments using human buffy coats were approved by the Humanitas Clinical and Research Institute IRB (approval 28/01/2016). All experiments using mice were conducted upon the approval of the Italian Ministry of Health (protocols 256/2015-PR for Humanitas and 803/2016-PR for San Raffaele Institutional Animal Care and Use Committees, IACUC) and NCI IACUC (protocol ETIB008).

Author contributions

KP, ES, and EL conceived the study. KP, ES, S. Puccio, FDP, GDS, MB, and VZ performed experiments. S. Polletti generated RNAseq libraries. S. Puccio and EMCM performed bioinformatic analysis. PDL and MI performed experiments with C57/BL6 mice. SG and LG performed tumor experiments with NSG mice. KP, ES, and EL analyzed and interpreted the data and wrote the manuscript. All authors edited the manuscript.

Acknowledgments

We wish to thank the members of the Laboratory of Translational Immunology for critical discussions. This work was supported by grants from the European Research Council (ERC-StG-2014 PERSYST 640511), the Fondazione Cariplo (grant Ricerca Biomedica 2012/0683), the Italian Ministry of Health (Bando Giovani Ricercatori GR-2011-02347324), the European Union Marie Curie Career Integration Grant (322093), and the Humanitas Clinical and Research Center (all to EL). KP and EMCM are recipients of the Fondazione Umberto Veronesi postdoctoral fellowships (2018 and 2017, respectively). ES and GDS are recipients of the Associazione Italiana per la Ricerca sul Cancro 3-year fellowships. Purchase of the BD FACSSymphony A5 has been in part defrayed by a grant from Italian Ministry of Health (agreement 82/2015).

Address correspondence to: Enrico Lugli, Laboratory of Translational Immunology, Humanitas Clinical and Research Center, Via Manzoni 113, 20089, Rozzano (MI), Italy. Phone: 39.02.8224.5143; Email: enrico.lugli@humanitasresearch.it.

1. June CH, et al. Engineered T cells for cancer therapy. *Cancer Immunol Immunother.* 2014;63(9):969–975.
2. Gardner R, et al. Acquisition of a CD19-negative myeloid phenotype allows immune escape of MLL-rearranged B-ALL from CD19 CAR-T-cell therapy. *Blood.* 2016;127(20):2406–2410.
3. Fraietta JA, et al. Determinants of response and resistance to CD19 chimeric antigen receptor (CAR) T cell therapy of chronic lymphocytic leukemia. *Nat Med.* 2018;24(5):563–571.
4. Gattinoni L, et al. Acquisition of full effector function in vitro paradoxically impairs the in vivo antitumor efficacy of adoptively transferred CD8+ T cells. *J Clin Invest.* 2005;115(6):1616–1626.
5. Shen X, et al. Persistence of tumor infiltrating lymphocytes in adoptive immunotherapy correlates with telomere length. *J Immunother.* 2007;30(1):123–129.
6. Gattinoni L, et al. Wnt signaling arrests effector T cell differentiation and generates CD8+ memory stem cells. *Nat Med.* 2009;15(7):808–813.
7. Gattinoni L, et al. A human memory T cell subset with stem cell-like properties. *Nat Med.* 2011;17(10):1290–1297.
8. Gattinoni L, Klebanoff CA, Restifo NP. Paths to stemness: building the ultimate antitumor T cell. *Nat Rev Cancer.* 2012;12(10):671–684.
9. Lugli E, et al. Superior T memory stem cell persistence supports long-lived T cell memory. *J Clin Invest.* 2013;123(2):594–599.
10. Mahnke YD, Brodie TM, Sallusto F, Roederer M, Lugli E. The who's who of T-cell differentiation: human memory T-cell subsets. *Eur J Immunol.* 2013;43(11):2797–2809.
11. Biasco L, et al. In vivo tracking of T cells in humans unveils decade-long survival and activity of genetically modified T memory stem cells. *Sci Transl Med.* 2015;7(273):273ra13.
12. Roberto A, et al. Role of naive-derived T memory stem cells in T-cell reconstitution following allogeneic transplantation. *Blood.* 2015;125(18):2855–2864.
13. Cieri N, et al. Generation of human memory stem T cells after haploidentical T-replete hematopoietic stem cell transplantation. *Blood.* 2015;125(18):2865–2874.
14. Klebanoff CA, et al. Central memory self/tumor-reactive CD8+ T cells confer superior antitumor immunity compared with effector memory T cells. *Proc Natl Acad Sci USA.* 2005;102(27):9571–9576.
15. Crompton JG, et al. Akt inhibition enhances expansion of potent tumor-specific lymphocytes with memory cell characteristics. *Cancer Res.* 2015;75(2):296–305.
16. van der Waart AB, et al. Inhibition of Akt signaling promotes the generation of superior tumor-reactive T cells for adoptive immunotherapy. *Blood.* 2014;124(23):3490–3500.
17. Kagoya Y, et al. BET bromodomain inhibition enhances T cell persistence and function in adoptive immunotherapy models. *J Clin Invest.* 2016;126(9):3479–3494.
18. Lugli E, et al. Identification, isolation and in vitro expansion of human and nonhuman primate T stem cell memory cells. *Nat Protoc.* 2013;8(1):33–42.
19. Cieri N, et al. IL-7 and IL-15 instruct the generation of human memory stem T cells from naive precursors. *Blood.* 2013;121(4):573–584.
20. Chapuis AG, et al. Transferred WT1-reactive CD8+ T cells can mediate antileukemic activity and persist in post-transplant patients. *Sci Transl Med.* 2013;5(174):174ra27.
21. Sabatino M, et al. Generation of clinical-grade CD19-specific CAR-modified CD8+ memory stem cells for the treatment of human B-cell malignancies. *Blood.* 2016;128(4):519–528.
22. Zanon V, et al. Curtailed T-cell activation curbs effector differentiation and generates CD8+ T cells with a naturally-occurring memory stem cell phenotype. *Eur J Immunol.* 2017;47(9):1468–1476.
23. Kondo T, et al. Notch-mediated conversion of activated T cells into stem cell memory-like T cells for adoptive immunotherapy. *Nat Commun.* 2017;8:15338.
24. Sukumar M, et al. Inhibiting glycolytic metabolism enhances CD8+ T cell memory and antitumor function. *J Clin Invest.* 2013;123(10):4479–4488.
25. Gattinoni L, Speiser DE, Lichterfeld M, Bonini C. T memory stem cells in health and disease. *Nat Med.* 2017;23(1):18–27.
26. MacIver NJ, Michalek RD, Rathmell JC. Metabolic regulation of T lymphocytes. *Annu Rev Immunol.* 2013;31:259–283.
27. Krauss S, Brand MD, Buttgerit F. Signaling takes a breath—new quantitative perspectives on bioenergetics and signal transduction. *Immunity.* 2001;15(4):497–502.
28. Pearce EL, et al. Enhancing CD8 T-cell memory by modulating fatty acid metabolism. *Nature.* 2009;460(7251):103–107.
29. van der Windt GJ, et al. Mitochondrial respiratory capacity is a critical regulator of CD8+ T cell memory development. *Immunity.* 2012;36(1):68–78.
30. O'Neill LA, Kishton RJ, Rathmell J. A guide to immunometabolism for immunologists. *Nat Rev Immunol.* 2016;16(9):553–565.
31. Geiger R, et al. L-Arginine modulates T cell metabolism and enhances survival and anti-tumor activity. *Cell.* 2016;167(3):829–842.e13.
32. Yang W, et al. Potentiating the antitumor response of CD8(+) T cells by modulating cholesterol metabolism. *Nature.* 2016;531(7596):651–655.
33. Buck MD, et al. Mitochondrial dynamics controls T cell fate through metabolic programming. *Cell.* 2016;166(1):63–76.
34. Sukumar M, et al. Mitochondrial membrane potential identifies cells with enhanced stemness for cellular therapy. *Cell Metab.* 2016;23(1):63–76.
35. Sena LA, et al. Mitochondria are required for antigen-specific T cell activation through reactive oxygen species signaling. *Immunity.*

- 2013;38(2):225–236.
36. Mak TW, et al. Glutathione primes T cell metabolism for inflammation. *Immunity*. 2017;46(4):675–689.
37. Zafarullah M, Li WQ, Sylvester J, Ahmad M. Molecular mechanisms of N-acetylcysteine actions. *Cell Mol Life Sci*. 2003;60(1):6–20.
38. Criddle DN, et al. Menadione-induced reactive oxygen species generation via redox cycling promotes apoptosis of murine pancreatic acinar cells. *J Biol Chem*. 2006;281(52):40485–40492.
39. Oberdoerffer S, Moita LF, Neems D, Freitas RP, Hacohen N, Rao A. Regulation of CD45 alternative splicing by heterogeneous ribonucleoprotein, hnRNPLL. *Science*. 2008;321(5889):686–691.
40. Araki K, et al. mTOR regulates memory CD8 T-cell differentiation. *Nature*. 2009;460(7251):108–112.
41. Sarbassov DD, Sabatini DM. Redox regulation of the nutrient-sensitive raptor-mTOR pathway and complex. *J Biol Chem*. 2005;280(47):39505–39509.
42. Tomasoni R, et al. Rapamycin-sensitive signals control TCR/CD28-driven Ifng, Il4 and Foxp3 transcription and promoter region methylation. *Eur J Immunol*. 2011;41(7):2086–2096.
43. Yang K, Chi H. mTOR and metabolic pathways in T cell quiescence and functional activation. *Semin Immunol*. 2012;24(6):421–428.
44. O'Sullivan D, et al. Memory CD8(+) T cells use cell-intrinsic lipolysis to support the metabolic programming necessary for development. *Immunity*. 2014;41(1):75–88.
45. Guidotti LG, et al. Immunosurveillance of the liver by intravascular effector CD8(+) T cells. *Cell*. 2015;161(3):486–500.
46. Singh N, Perazzelli J, Grupp SA, Barrett DM. Early memory phenotypes drive T cell proliferation in patients with pediatric malignancies. *Sci Transl Med*. 2016;8(320):320ra3.
47. Xu Y, et al. Closely related T-memory stem cells correlate with in vivo expansion of CAR.CD19-T cells and are preserved by IL-7 and IL-15. *Blood*. 2014;123(24):3750–3759.
48. Utzschneider DT, et al. T cell factor 1-expressing memory-like CD8(+) T cells sustain the immune response to chronic viral infections. *Immunity*. 2016;45(2):415–427.
49. Scheffel MJ, et al. Efficacy of adoptive T-cell therapy is improved by treatment with the antioxidant *n*-acetyl cysteine, which limits activation-induced T-cell death. *Cancer Res*. 2016;76(20):6006–6016.
50. Scheffel MJ, et al. N-acetyl cysteine protects anti-melanoma cytotoxic T cells from exhaustion induced by rapid expansion via the downmodulation of Foxo1 in an Akt-dependent manner. *Cancer Immunol Immunother*. 2018;67(4):691–702.
51. Bigarella CL, Liang R, Ghaffari S. Stem cells and the impact of ROS signaling. *Development*. 2014;141(22):4206–4218.
52. Aruoma OI, Halliwell B, Hoey BM, Butler J. The antioxidant action of N-acetylcysteine: its reaction with hydrogen peroxide, hydroxyl radical, superoxide, and hypochlorous acid. *Free Radic Biol Med*. 1989;6(6):593–597.
53. Samuni Y, Goldstein S, Dean OM, Berk M. The chemistry and biological activities of N-acetylcysteine. *Biochim Biophys Acta*. 2013;1830(8):4117–4129.
54. Lugli E, Zanon V, Mavilio D, Roberto A. FACS analysis of memory T lymphocytes. *Methods Mol Biol*. 2017;1514:31–47.
55. Irizarry RA, et al. Exploration, normalization, and summaries of high density oligonucleotide array probe level data. *Biostatistics*. 2003;4(2):249–264.
56. Subramanian A, et al. Gene set enrichment analysis: a knowledge-based approach for interpreting genome-wide expression profiles. *Proc Natl Acad Sci USA*. 2005;102(43):15545–15550.
57. Picelli S, Björklund ÅK, Faridani OR, Sagasser S, Winberg G, Sandberg R. Smart-seq2 for sensitive full-length transcriptome profiling in single cells. *Nat Methods*. 2013;10(11):1096–1098.
58. Dobin A, et al. STAR: ultrafast universal RNA-seq aligner. *Bioinformatics*. 2013;29(1):15–21.
59. Robinson MD, McCarthy DJ, Smyth GK. edgeR: a Bioconductor package for differential expression analysis of digital gene expression data. *Bioinformatics*. 2010;26(1):139–140.
60. Conlon KC, et al. Redistribution, hyperproliferation, activation of natural killer cells and CD8 T cells, and cytokine production during first-in-human clinical trial of recombinant human interleukin-15 in patients with cancer. *J Clin Oncol*. 2015;33(1):74–82.